RSC Advances

RSC Publishing

PAPER

View Article Online
View Journal | View Issue

Diverting phase transition of high-melting-point stearic acid to room temperature by microencapsulation in boehmite†

Cite this: *RSC Adv.*, 2013, **3**, 22326

Lin Pan,[a] Qi Ji,[b] Yuwei Qin,[c] Yingchang Jiang,[a] Zhongping Zhang,[a] Shudong Zhang*[a] and Zhenyang Wang*[a]

Organic phase change materials (OPCMs) have long been recognized as potentially reversible thermal energy storage candidates due to their ability to reversibly store or release large amounts of latent heat when changing from one physical state to another. For application of which in solar heat storage, reducing their relatively high phase transition temperature (T_C) to room temperature is still challenging. Herein, a microemulsion with metastable interface is adopted for *in situ* synthesis of sphere-like structure stearic acid (SA)@boehmite (γ-AlOOH) microcapsules. Interestingly, when the high-melting-point SA crystals (T_C = 70.8 °C) were capsulated into boehmite nanoshells, their phase transition could be diverted to room temperature (~21 °C), which means about 50 °C decrease of their phase change temperature has been achieved. This dramatic change could be due to a confinement effect on the interface between SA cores and the boehmite nanoshells, which leads to a change of geometric factors and enhancement of shell-SA interactions. Furthermore, the heat energy storage density (~140 kJ kg^{-1}) of the obtained SA@γ-AlOOH microcapsules is higher than that of most common room temperature PCMs, suggesting an efficient heat storage ability. This kind of shape-stabilized microcapsule can be considered as candidate room temperature PCMs for thermal energy storage.

Received 26th July 2013
Accepted 20th September 2013

DOI: 10.1039/c3ra43936d

www.rsc.org/advances

Introduction

A phase change material (PCM) possesses the ability to absorb and release great amounts of energy in the form of latent heat (ΔH) during phase transitions between solid–solid or solid–liquid phases over a certain temperature range. Among the various interest heat storage techniques, the use of PCMs is particularly attractive due to their capability of having a high density, enabling a compact energy storage system at nearly isothermal conditions, and a high fusion heat.[1–3] Depending on the type of applications, the organic PCMs should first be selected based on their phase change temperature because a large number of organic PCMs are available in the temperature range from −5 °C to 190 °C.[4–8] And the organic PCMs and their mixtures that show phase change around 18–65 °C are suitable for the thermal comfort applications in textiles and in buildings.[9a] For example, hexadecane and octadecane,[9b] which have high energy storage density and phase transition near room temperatures, are very good paraffin candidates for energy storage purpose. However, the high price of paraffin candidates hinder to be widely applied in thermal storage technology (section S1, ESI†). Cheaper fatty acids have been recommended as one of the most important thermal energy storage materials due to their high energy storage density (150–230 kJ kg^{-1}) and desirable thermal and heat transfer characteristics[10,11](section S1, ESI†). Unfortunately, high phase transition temperature of fatty acids is not easy to be used directly in room temperature thermal energy storage applications such as building heating/cooling and indoor temperature control. How to reducing high T_C of fatty acids to near room temperature for improving to save thermal properties is still challenging.

Over the past decades, how to modify the T_C of PCM is an important research focus on material scientists and the field of energy saving. It is well known that confined PCMs at the nanometer size scale is one of the most effective ways to change T_C because of the presence of finite size and reduced dimensionality.[12–17] As all known, small confined particles have lower phase change point (melting point) than bulk materials due to an increased proportion of surface atoms as the size of particles

[a]*Institute of Intelligent Machines, Institution Chinese Academy of Sciences, Hefei, Anhui, 230031, P. R. China. E-mail: sdzhang@iim.ac.cn; zywang@iim.ac.cn; Fax: +86-551-65591156*

[b]*School of Physics and Engineering, Zhengzhou University, Zhengzhou, Henan, 450052, P. R. China*

[c]*School of Physics and Electrical Engineering, Weinan Normal University, Weinan, 714000, P. R. China*

† Electronic supplementary information (ESI) available: Thermophysical properties of PCMs, XRD patterns, DSC thermogram, and TGA of pristine SA, AlOOH and SA@AlOOH microcapsules. See DOI: 10.1039/c3ra43936d

decreases. The size-dependent phase change point depression of confined nanoparticles has been described in a classical thermodynamic approach by the so-called Gibbs–Thomson equation (eqn (1)).

$$\Delta T_C = T_{C,confined} = T_{C,bulk} = 2\frac{(\gamma_{wf} - \gamma_{ws})\nu}{H\lambda_{C,bulk}} \quad (1)$$

According to the Gibbs–Thomson thermodynamic equation (eqn (1)),[18–20] the shift of the phase transition temperature ΔT_C is inversely proportional to the pore radius H and is proportional to the difference of the surface tension $\gamma_{wf} - \gamma_{ws}$, where γ_{wf} and γ_{ws} are the wall-fluid surface tensions, ν is the molar volume of the liquid phase and $\lambda_{c,bulk}$ is the bulk latent heat of fusion. In the previous confined system including cylindrical, subnanometer pores, films and porous materials,[18–24] most confined size is various nanoscale confined systems, these efforts have met with many limitations including small binding capacity, slow mass transfer, and irregular materials shape. One of main reasons is that the insert of PCM into interior area of confined materials is quite difficult due to the high capillary pressure nature of nanopores in nanoscale confined systems.

Compared with nanoscale confined systems, the most significant advantages of microencapsulated PCMs are mechanical/chemical stability, low cost, and ease of preparation, and hence have attracted extensive research interest.[25–29] And microcapsules offer thin closed structure within a restricted diameter range, and their internal van der Waals surfaces will regulate the phase change behavior of encapsulated PCMs in a precise fashion. The structure of PCMs results from a balance between short-range geometric factors and high pressure inside microcapsules compared to the unconfined state. In addition, their overall micrometer-sized structure not only possesses a robust and strong mechanical structure that can prevent PCM leakage for extended periods of time in the cycling process but also provides the necessary mechanical robustness against wear and tear in the fabrication process of the heat storage unit.

Herein, a metastable interface of microemulsion method is proposed for *in situ* synthesis of sphere-like structure stearic acid (SA)@γ-AlOOH microcapsules. Interestingly, high-melting-point SA crystal (T_C = 70.8 °C) coated into nanocavities of γ-AlOOH could be able to observation of room temperature thermal transitions (~21 °C) by differential scanning calorimetry (DSC). The transition temperature of SA coated in γ-AlOOH shells was determined by confinement effect leading to change geometric factors and enhancement of shell-SA interactions. Furthermore, the heat energy storage density of obtained SA@γ-AlOOH samples is very closer the near room temperature PCM. Due to its excellent thermal stability and reliability and simple preparation method, the shape-stabilized SA@γ-AlOOH microcapsule can be considered as candidate PCMs for thermal energy storage applications.

Experimental section

Materials

All chemical agents were of analytical grade purity obtained from Shanghai Chemicals Ltd. and directly used as received without further purification. And deionized water with a resistivity of 18.2 MΩ was used.

1. Preparation of SA@γ-AlOOH (21.6 wt% of SA) microcapsules (sample no. S1). Stearic acid (SA)@γ-AlOOH microcapsules were prepared using an *in situ* emulsion precipitation method. Typically, stearic acid (SA, 0.1 g) and the n-amyl alcohol (NAA, 1.5 mL) were dissolved in deionized H_2O (35 mL) in a 100 mL flask at 78 °C. Then, anionic surfactant sodium dodecyl sulfate (SDS, 0.5 g) was added into the above solution for a metastable microemulsion under stirring of 40 min. Next, acid $AlCl_3$ solution (0.1 g of $AlCl_3 \cdot 6H_2O$ dissolved in 15 mL of deionized H_2O) was dropwise added into the flask. After stirring for 30 min at 78 °C, the white precipitation was initiated by dripping of $NaHCO_3$ aqueous solution (0.2 g of $NaHCO_3$ dissolved in 15 mL deionized H_2O) to increase pH value of the microemulsion. The hydrolysis reaction was kept at 78 °C for 1 h. The resultant products were purified by centrifugation for several times to remove some unreacted reagents and dried at 40 °C for 24 h under vacuum oven.

2. Preparation of SA@γ-AlOOH (28.5 wt% of SA) (sample no. S2) and SA@γ-AlOOH (39 wt% of SA) microcapsules (sample no. S3). The synthetic procedure was similar to that of the SA@γ-AlOOH (21.6 wt% of SA) microcapsules except that the amounts of stearic acid were changed to 0.2 g and 0.3 g, respectively.

Characterization

The morphology of the obtained SA@γ-AlOOH microcapsules was investigated by field emission scanning electron microscopy (FESEM, FEI 200) and transmission electron microscopy (TEM, JEOL 2010), respectively. The phase structure of the SA@γ-AlOOH microcapsules was determined by using X-ray diffraction (XRD) pattern, which was recorded on a Rigaku Dmax diffraction system using a Cu Kα source (λ = 1.54187 Å). The spectroscopic analyses of microcapsules were per-formed on a KBr disk using an IR instrument (Thermo-Fisher Nicolet is10 FTIR spectrometer). Raman spectra were obtained using the DXR confocal microscopy Raman system (Thermo Fisher Scientific Inc. Waltham, MA) with a 10× air objective with a 532 nm excitation laser with a 50 μm slit for confocality. The laser power and accumulation time were 10 mW and 5 s, respectively. Thermal properties of microcapsules such as melting and crystallizing points and latent heats were measured by DSC technique (Netzsh model DSC 200).

Results and discussion

Scheme 1 describes the simple procedure for *in situ* synthesizing the SA@γ-AlOOH microcapsules. A variable amount of SA is dissolved in NAA and H_2O for the formation of solution. Subsequently, when anionic surfactant SDS is introduced into the above solution, the hydrophilic negatively charged groups formed on micelles around the surface of the SA micro droplets as the polar water and nonpolar NAA do not dissolve into each other. Then, when acid $AlCl_3$ solution was dropwise added, the strong electrostatic forces between the Al^{3+} and negatively

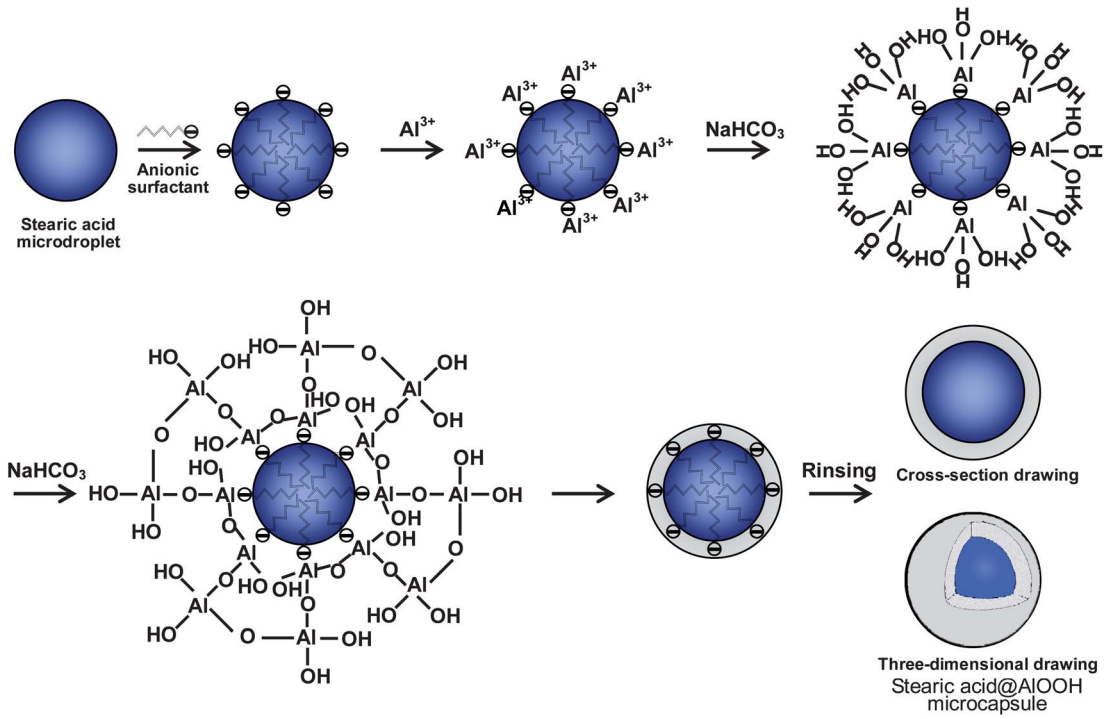

Scheme 1 A schematic illustration of the formation process of SA@γ-AlOOH microcapsules structure.

charged groups at the surface of the SA micro droplets will thus drive the selective absorption at the surface of the SA micro droplets. Therefore, γ-AlOOH nuclei firstly form on the interface of vesicles from hydrolysis reaction of Al^{3+} in SA droplets attributed to increasing pH value of solution by introducing of $(NH_3)_2HCO_3$. Afterwards, Al–O–Al net structure generated with dehydration reaction of Al–OH in alkaline solution, and thus, a γ-AlOOH shell is successfully fabricated onto the surface of the SA droplets though this polycondensation process.

We demonstrated the above synthesis concept by experimental examples, as shown in the scanning electron microscopy (SEM) and transmission electron microscopy (TEM) images of Fig. 1a–c. The low magnification SEM image (Fig. 1a) shows that this sample mainly consists of SA@γ-AlOOH microspheres having diameters of 250–700 nm. The high magnification SEM image (upper inset of Fig. 1a) of SA@γ-AlOOH microsphere shell shows that the shells have smooth surface and high compactness. Fig. 1b and c shows the TEM image of core–shell microspheres of SA@γ-AlOOH with a uniform shell thickness of *ca.* 85 nm and 60 nm, respectively, measured from the change of particle sizes. Meanwhile, both SA and shells can simultaneously be observed by high-magnification TEM (upper inset of Fig. 1b and c). The thickness of AlOOH shells decreased with the amount of SA, and they are tunable from ~85 to 20 nm (Fig. 1b and c and S1, ESI†).

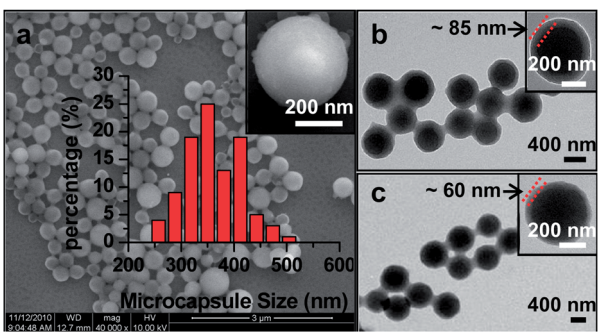

Fig. 1 Typical SEM and TEM images of the obtained SA@AlOOH samples. (a) Low-magnification and high-magnification (upper inset) SEM images and size distribution (bottom inset) of SA@γ-AlOOH (21.6 wt% of SA) microcapsules. Low-magnification and high-magnification (upper inset) TEM images of SA@γ-AlOOH (21.6 wt% of SA) microcapsules (b) and SA@γ-AlOOH (28.5 wt% of SA) microcapsules (c).

Differential scanning calorimetry (DSC) is very suitable technique to study phase transformation of a PCM confined inside the microcapsules. Results of DSC experiments with samples of SA@γ-AlOOH microcapsules with different content of SA were shown in Fig. 2. The DSC scan for the pure SA sample presented an endothermic peak at 70.8 °C for a melting temperature of SA, and no transition was observed for the γ-AlOOH in this entire temperature region (Fig. 2a). In contrast, SA@γ-AlOOH (sample no. S1, S2, and S3) clearly exhibited a transition at 21.6, 29.7, and 31.6 °C (Table 1), respectively, which are considerably lower than the melting temperature of neat SA (Fig. 2a). This results suggested that high-melting-point SA (T_C = 70.8 °C) coated into nanocavities of γ-AlOOH could be able to reduce near room temperature thermal transitions (~21 °C). The transition temperature of SA coated in γ-AlOOH shells may be determined by confinement effect leading to change geometric factors and enhancement of shell–SA interactions. Meanwhile, we further confirmed that the transition temperature of SA coated in γ-AlOOH shells could be able to

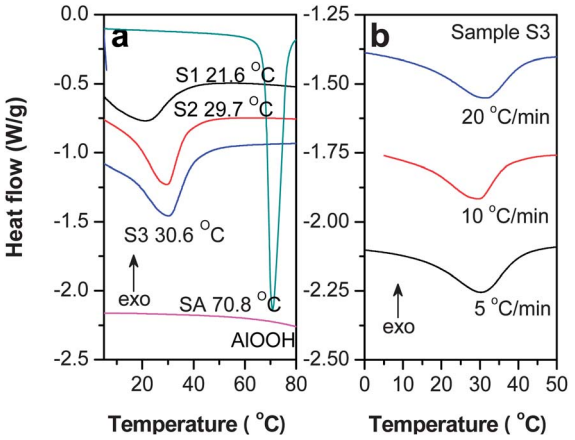

Fig. 2 (a) DSC thermogram of the pure SA, γ-AlOOH and the as-prepared SA@γ-AlOOH microcapsules with a heating rate of 10 °C min^{-1}, respectively. (b) DSC thermogram of the as-prepared SA@γ-AlOOH (39 wt% of SA) microcapsules with a different heating rate of 5, 10 and 20 °C min^{-1}, respectively.

Table 1 SA encapsulation ratios (M), melting temperature (T_m), melting enthalpy values (ΔH_{MEPEM}), thermal storage capability ratios (η_{PCM}) and total thermal storage efficiency (η_{Total})for pure SA, sample S1, S2 and S3, respectively

Sample	M	T_m (°C)	ΔH_{MEPEM} (kJ kg^{-1})	η_{PCM}	η_{Total}
SA	100%	70.8	270.2	100%	100%
S1	21.6%	21.6	137.96	51.06%	11.03%
S2	28.5%	29.7	143.86	53.24%	15.17%
S3	39%	30.6	124.36	46.02%	17.95%

reduce near room temperature on thermal analysis with a different heating rate of 5, 10 and 20C min^{-1}, respectively (Fig. 2b). The same thermal analysis results were also observed in the other products of SA@γ-AlOOH microcapsules.

The shell and core phase of the obtained microcapsules were examined by X-ray diffraction (XRD) (Fig. 3) at room temperature. The sharp peak at 14.5° can be clearly matched the main (020) peak of orthorhombic γ-AlOOH (JCPDS card no. 74-1895), implying that the shell of microcapsules was γ-AlOOH phase. The broad diffraction peak around 21° in XRD pattern is ascribed to (110) peak of α-stearic acid (JCPDS card no. 09-0618). Compare with the sample of no. S1 and S2, only no. S3 of SA@γ-AlOOH had a broad diffraction peak at room temperature (Fig. 3a). All the obtained samples appeared a weak and broad (110) peak of α-stearic acid phase around 21° in XRD pattern when the samples were kept in the ~5 °C refrigerator (Fig. 3b). Those results were shown that cooling of the SA@γ-AlOOH samples of no. S1 and S2 resulted in a clear phase transition, which is lower than the freezing point of pure SA. After SA confined in γ-AlOOH shells, the strong and sharp diffraction peak from the pure SA (Fig. S2, ESI†) was displaced with the weak and broad (110) peak from SA confined in γ-AlOOH microcapsules. XRD analysis further confirmed that the SA in the interior of γ-AlOOH microcapsules became a short-range order than the high-melting-point pure SA crystals (Fig. S2 and S3a, ESI†). Also, the above XRD results were all in good agreement with the DSC analysis.

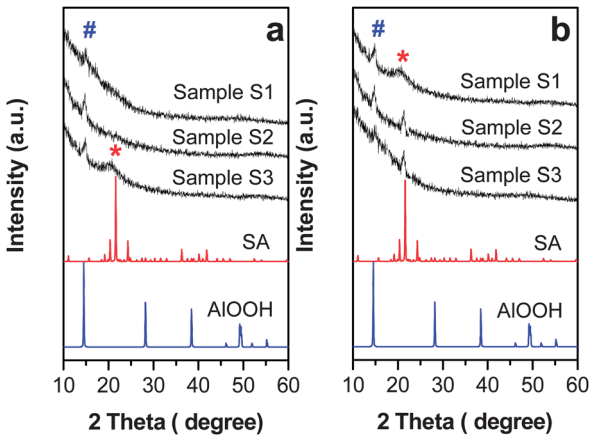

Fig. 3 (a) The experimental XRD pattern (peaks generated by AlOOH and SA are marked with # and * symbol, respectively) of the SA@AlOOH powders at room temperature (~25 °C). (b) The corresponding XRD pattern of the freezed SA@AlOOH powders. The standard pattern of blue line in JCPDS card no. 74-1895 for AlOOH and red line in ICPDS card no. 09-0618 for pure SA.

Based on the Gibbs–Thomson thermodynamic equation, the shift in phase transition temperature T_C can be related to not only the pore width (H) but host–guest interactions under the confinement condition. And such host–guest interaction is an important influence factor on the phase transition temperature of PCM. For example, polymer host and polyethylene glycol (PEG) guest interactions cause a huge decrease in the PEG phase change temperature to induce the solidification of PEG assembly.[22] The host–guest interaction characteristic of the microcapsules was carried out using IR spectroscopy method. Fig. 4 shows the FTIR spectra of pure SA, γ-AlOOH and SA@γ-AlOOH samples, respectively. The intensive band around 3450 cm^{-1} belongs to the Al–O–H stretching vibration, as shown in Fig. 4. The interaction between SA and γ-AlOOH crystals has also been verified by the shift of C=O stretching band of SA originally at ~1700 cm^{-1} to a lower frequency of ~1590 cm^{-1} in the FTIR spectra. The observable frequency shifts of the main C=O group of SA means that there are strong interface interactions between the COOH group of the SA and alkaline region

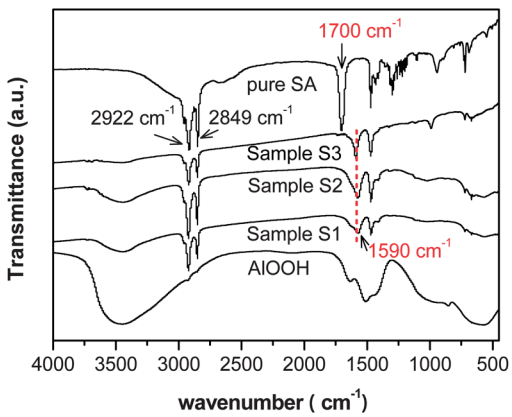

Fig. 4 FTIR spectra of pure SA, AlOOH and SA@AlOOH samples, repectively.

in AlOOH, which can change the thermal physical properties of encapsulated SA.

Heat storage capacity is a very important reference index for measure of the PCM heat storage performance. The thermal storage capabilities of microcapsules were calculated by eqn (2).

$$\eta_{\mathrm{MEPCM}} = \frac{\frac{\Delta H_{\mathrm{Total}}}{M}}{\Delta H_{\mathrm{PCM}}} \times 100\% = \frac{\Delta H_{\mathrm{MEPCM}}}{\Delta H_{\mathrm{PCM}}} \times 100\% \quad (2)$$

where η_{MEPCM} is thermal storage capability rate of the microcapsule, $\Delta H_{\mathrm{Total}}$ is total enthalpy values of microcapsules, ΔH_{PCM} is enthalpy values of pure PCM, and M is the encapsulating ratio of PCM.[18,22]

The quantification of SA molecule content in the SA@γ-AlOOH samples was easily confirmed by normalizing the thermogravimetric analysis (TGA) curves of the microcapsules to those of the respective pure SA (Fig. S4, ESI†), because not all of the initially dissolved SA molecules were retained in the fabricated microcapsules. These TGA results (Table 1) clearly demonstrate that high content of SA could be encapsulated into the interior of the γ-AlOOH microcapsules, which encapsulation ratios (M) for the S1, S2 and S3 were 21.6%, 28.5% and 39%, respectively. The latent heats of melting (ΔH) were 29.8, 41.0, 48.5 and 270.2 J g^{-1} for S1, S2, S3 and SA, respectively, shown in Table 1. Thermal storage capabilities of S1, S2 and S3 are calculated as 137.96, 143.86 and 124.36 J g^{-1}, respectively, and thermal storage capability rate (η_{PCM}) is 51.06%, 53.24%, and 46.02% (Table 1), respectively. Those results demonstrated that the heat energy storage density of obtained SA@γ-AlOOH is very closer the near room temperature PCM (section S1, ESI†). For encapsulated energy storage applications, when calculating the storage efficiency, the weight of matrix material can't be ignored, because the energy storage capacity is also volume related. The total thermal storage efficiency of microcapsules were calculated by eqn (3). The total thermal storage efficiency (η_{Total}) is 11.03%, 15.17%, and 17.95% (Table 1), respectively.

$$\eta_{\mathrm{Total}} = \frac{\Delta H_{\mathrm{Total}}}{\Delta H_{\mathrm{PCM}}} \times 100\% \quad (3)$$

Conclusions

In conclusion, we have demonstrated a metastable in-terface of microemulsion method for *in situ* synthesis of sphere-like structure stearic acid (SA)@boehmite (γ-AlOOH) microcapsules. Reversible phase transition of SA from high melting point to temperature near ambient in as-prepared SA@γ-AlOOH microcapsules was successfully achieved through a microencapsulation confinement method. Furthermore, the obtained SA@γ-AlOOH microcapsules still have a high heat energy storage density. Our results not only provide a good example to the development of new types of heat energy storage composite materials, but they also are helpful for the understanding of phase transitions of dimensionally confined environments and the related phenomena within the nanoscale confines.

Acknowledgements

The authors would like to thank the National Basic Research Program of China (no. 2009CB939902), National Natural Science Foundation of China (no. 51202253, 51002159).

Notes and references

1 M. M. Farid, A. M. Khudhair, S. A. K. Razack and S. Al-Hallaj, *Energy Convers. Manage.*, 2004, **45**, 1597–1615.
2 S. Mondal, *Appl. Therm. Eng.*, 2008, **28**, 1536–1550.
3 A. M. Borreguero, J. L. Valverde, T. Peijs, J. F. Rodrıguez and M. Carmona, *J. Mater. Sci.*, 2010, **45**, 4462–4469.
4 J. K. Choi, J. G. Lee, J. H. Kim and H. S. Yang, *J. Ind. Eng. Chem.*, 2001, **7**, 358–362.
5 C. Alkan, *Thermochim. Acta*, 2006, **451**, 126–130.
6 B. Zalba, J. Maŕin, L. F. Cabeza and H. Mehling, *Appl. Therm. Eng.*, 2003, **23**, 251–283.
7 V. V. Tyagi and D. Buddhin, *Renewable Sustainable Energy Rev.*, 2007, **11**, 1146–1166.
8 A. Agbossou, Q. Zhang, G. Sebald and D. Guyomar, *Sens. Actuators, A*, 2010, **163**, 277–283.
9 (*a*) D. Feldman, M. M. Shapiro and D. Banu, *Sol. Energy Mater.*, 1986, **13**, 1–10; (*b*) S. G. Jeong, J. Jeon, J. H. Lee and S. Kim, *Int. J. Heat Mass Transfer*, 2013, **62**, 711–717.
10 L. Pan, Q. H. Tao, S. D. Zhang, S. S. Wang, J. Zhang, S. H. Wang, Z. Y. Wang and Z. P. Zhang, *Sol. Energy Mater. Sol. Cells*, 2012, **98**, 66–70.
11 B. X. Li, T. X. Liu, L. Y. Hu, Y. F. Wang and S. B. Nie, *Chem. Eng. J.*, 2013, **215–216**, 819–826.
12 V. C. Holmberg, M. G. Panthanl and B. A. Korgel, *Science*, 2009, **326**, 405–407.
13 B. J. Kim, J. Tersoff, S. Kodambaka, M. C. Reuter, E. A. Stach and F. M. Ross, *Science*, 2008, **322**, 1070–1073.
14 C. J. Ekkusib and J. M. Torkelson, *Nat. Mater.*, 2003, **2**, 695–700.
15 G. B. DeMaggio, W. E. Frieze, D. W. Gidley, M. Zhu, H. A. Hristov and A. F. Yee, *Phys. Rev. Lett.*, 1997, **78**, 1524–1527.
16 A. Bansal, H. Yang, C. Z. Li, K. Cho, B. C. Benicewicz, S. K. Kumar and L. S. Schaldler, *Nat. Mater.*, 2005, **4**, 693–698.
17 P. Rittigstein, R. D. Priestley, L. J. Broadbelt and J. M. Torkelson, *Nat. Mater.*, 2007, **6**, 278–282.
18 M. Alcoutlabi and G. B. McKenna, *J. Phys.: Condens. Matter*, 2005, **17**, R461–R524.
19 J. Warnock, D. D. Awschalom and M. W. Shafer, *Phys. Rev. Lett.*, 1986, **57**, 1753–1756.
20 R. Evans and U. Marini Bettolo Marconi, *J. Chem. Phys.*, 1987, **86**, 7138–7148.
21 C. Alba-Simionesco, B. Coasne, G. Dosseh, G. Dudziak, K. E. Gubbins, R. Radhakrishnan and M. Sliwinska-Bartkowiak, *J. Phys.: Condens. Matter*, 2006, **18**, R15–R68.
22 T. Uemura, N. Yanai, S. Watanabe, H. Tanaka, R. Numaguchi, M. T. Miyahara, Y. Ohta, M. Nagaoka and S. Kitagawa, *Nat. Commun.*, 2010, **1**, 1–8.
23 S. D. Zhang, Q. H. Tao, Z. Y. Wang and Z. P. Zhang, *J. Mater. Chem.*, 2013, **22**, 20166–20169.

24 S. J. You, S. Luzan, J. C. Yu, B. Sundqvist and A. V. Talyzin, *J. Phys. Chem. Lett.*, 2012, **3**, 812–817.
25 Y. Rong, H. Z. Chen, D. C. Wei, J. Z. Sun and M. Wang, *Colloids Surf., A*, 2004, **242**, 17–20.
26 K. Hong and S. Park, *Mater. Sci. Eng., A*, 1999, **272**, 418–421.
27 H. Z. Zhang, X. D. Wang and D. Z. Wu, *J. Colloid Interface Sci.*, 2010, **343**, 246–255.
28 J. S. Cho, A. Kwon and C. G. Cho, *Colloid Polym. Sci.*, 2002, **280**, 260–266.
29 O. Pascu, R. Garcia-Valls and M. Giamberini, *Polym. Int.*, 2008, **57**, 995–1006.